Molecular mechanisms of seasonal brain shrinkage and regrowth in *Sorex araneus*

William R. Thomas[1]*†, Dina K. N. Dechmann[2,3], John Nieland[4], Cecilia Baldoni[2,3], David Carlson[1], Dominik von Elverfeldt[5], Julie Holm-Jacobsen[4], Marion Muturi[2], Angelique Corthals[6]‡, Liliana M. Dávalos[1,7]‡*

[1]Department of Ecology and Evolution, Stony Brook University; Stony Brook, NY 11794, United States.

[2]Max-Planck Institute for Animal Behavior; Radolfzell, 78315, Germany.

[3]University of Konstanz; Konstanz, 78464, Germany.

[4]Health Science and Technology, Aalborg University; Aalborg, 9100, Denmark.

[5]Division of Medical Physics, Department of Diagnostic and Interventional Radiology, University Medical Center Freiburg, Faculty of Medicine, University of Freiburg, Freiburg, Germany.

[6]John Jay College of Criminal Justice; New York, NY 10019, United States.

[7]Consortium for Inter-Disciplinary Environmental Research, Stony Brook University; Stony Brook, NY 11794, United States.

† Lead author

‡ These authors contributed equally to this work

* Corresponding authors: William R. Thomas and Liliana M. Dávalos

Emails: William.thomas@stonybrook.edu, Liliana.Davalos@stonybrook.edu

Author Contributions: LD, DD, AC, and JN conceived and funded project. CB, MM, and DD collected, measured, and sampled shrews. WRT designed and conducted genomic analyses. WRT, JHJ, JN, and AC analyzed metabolite concentrations. WRT visualized data and wrote initial draft. LD, DD, JN, DC, and AC contributed to review and editing of draft. All authors contributed to data interpretation.

Competing Interest Statement: Authors disclose no competing interests.

Keywords: Dehnel's phenomenon, neurodegeneration, winter, metabolism, shrew

Abstract

Mammalian brains typically grow through development. In contrast, the Eurasian common shrew *Sorex araneus* has evolved a wintering strategy that shrinks many organs in autumn, including their brain, then rapidly regrow in spring. To explore the molecular underpinnings of this unique brain size change, we analyzed multi-organ, season-specific transcriptomics and metabolomic data. Simultaneous with brain shrinkage, we discovered system-wide metabolic shifts from lipid to glucose metabolism, similar to hypoxia responses, as well as neuroprotection of brain metabolic homeostasis through reduced cholesterol efflux. Analyses of co-expression models uncovered a finely tuned brain-liver crosstalk underlying these shifts, with the brain shrinkage module comprising of markers associated with longevity-regulating pathways and pathways involved in neurodegeneration, including Parkinson's disease and Huntington's disease. We propose metabolic shifts are central to seasonal brain size changes in *S. araneus*, with potential implications for mammalian neurodegeneration and neuroregeneration.

Main Text

Introduction

Animals vary widely in their wintering adaptations. The most common ones are hibernation or migration, but a handful of species that cannot migrate or slow their metabolism have evolved wintering size plasticity: Dehnel's phenomenon (DP) (*1*, *2*). This pattern of growth, best studied in the Eurasian common shrew, *Sorex araneus*, is unlike that of almost every other mammal. Instead of growing continuously to adulthood, juvenile *S. araneus* grow to an initial maximum size in the first summer of their disproportionately brief life (~1 year). Shrews then shrink, reaching a nadir in winter, followed by rapid regrowth to their adult, breeding size in spring. This size plasticity also occurs in the brain, with a 26% volume decrease through winter and in contrast with typical unidirectional brain growth in mammals (*2*). In spring, the brain then partially regrows. Although DP has garnered much interest because of its potential for regenerating organs, especially the brain, the molecular underpinnings of this wintering adaptation remain largely unknown (*3*).

Dehnel's phenomenon corresponds to the unique physiological constraints shrews face. *S. araneus* have one of the highest mammalian metabolic rates measured to date (*4*), requiring high and constant food intake throughout the year. Research on shrew physiology has shown fat turnover in *S. araneus* is constantly high, with 50% turnover rates increasing from 4.5 hour in summer juveniles to 2.5 hours in winter (*5*). Yet, the amount of stored lipids in the liver is also highest during the winter months (*6*). Meanwhile, energy consumption per unit mass remains constant year-round (*7*). Given these high energy demands and high lipid turnover, DP is construed as an adaptation that compensates for the scarcity of resources in winter by reducing body size, particularly of energy-expensive tissue such as the brain (*5*, *8*). In humans, the brain accounts for 20% of glucose metabolized (*9*), and contains 25% of the unesterified cholesterol found in the body (*10*). But this high metabolic demand also makes the human brain vulnerable: metabolic changes have been implicated in the onset of human neurodegeneration (*11–13*). Therefore, we hypothesized that molecular changes underlying seasonal size change in shrew size may parallel those previously identified implicated in neurodegenerative diseases.

Changes in glucose and lipid metabolism have also been identified in hibernation (*14*, *15*), and Dehnel's phenomenon could share some of those regulatory mechanisms, which include reduced feeding, thermoregulation and hypoxia. Mechanistic analyses of mammalian hibernation have identified a toolkit of genes that regulates vast metabolic changes (*14–16*) associated with metabolic pathways, circadian rhythm, thermogenesis, and feeding behavior (*17*). For example, research across different species of hibernators has identified increased fatty acid oxidation simultaneous with downregulation of genes associated with the breakdown of glucose as a molecular metabolic switch underlying winter energy savings (*16*). Notably, these metabolic changes can have profound negative effects on the brain, specifically hypoxia (*18*). Thus, evolved neuroprotective responses to mitigate the harmful effects of metabolic fluctuations have been discovered in hibernating mammals (*19*, *20*). In the Arctic ground squirrel, the negative consequences of oxidative stress and glucose deprivation through hibernation are diminished by modifying neural ion channels (*21*). But *S. araneus* remain awake throughout the winter and thus experience a changing and metabolically demanding environment. To enable winter survival while maintaining activity, shrews are therefore likely to exhibit different regulatory patterns for metabolic functions suppressed in hibernators.

Metabolic changes associated with hibernation also show similarities to the metabolic dysregulation found in human neurodegenerative diseases. Both high fat and high sucrose diets have negative consequences on memory, mood, and other cognitive processes, akin to changes in lipid and glucose utilization under hibernation (*22*). Rats fed diets high in saturated fats and sugars perform worse in place recognition tests and exhibit higher oxidative stress and inflammation markers in the hippocampus (*23*, *24*). This occurs despite the protective functions of the blood-brain barrier (BBB), a semipermeable system of blood vessels that regulate the

entrance of molecules into the brain (*25*), insulating the brain from metabolic changes. In humans, BBB permeability increases with age, leading to diminished protection from metabolic shifts (*26*) and neurodegenerative diseases (*27*, *28*). Metabolic molecules that can cross the BBB, such as insulin and glucose (*29*), can thus have large effects on the brain. Circulating insulin and glucose increase in diseases such as type-2 diabetes and obesity, is associated with reduced brain size, motor activity, functional connectivity, and increased risk of developing Alzheimer's and Parkinson's diseases (*11–13*, *30*). As in both hibernation and human neurodegenerative disease, brain shrinkage and regrowth phenotypes may therefore be associated with metabolic shifts and transport of circulating molecules to the brain through the BBB.

To explore the metabolic hypothesis and its potential parallels, we collected phenotypic, metabolomic, and transcriptomic data from a shrew population across seasons, examining gene expression dynamics change throughout the entirety of DP size plasticity. We focused on: 1) blood, which circulates metabolites across the organisms, 2) liver, where many functions that regulate metabolism take place, including glucose processing, and 3) brain, where the anticipatory and predictable changes in volume occur. Our results show that shrews survive the winter through processes that in model organisms are pathological, while avoiding detrimental health effects. Our analyses reveal an unequivocal metabolic basis for DP, with implications for metabolic- and age-related human neurodegeneration.

Results

Confirming Dehnel's phenomenon in the German shrew population

Comparisons of body and organ mass throughout the cycle confirmed patterns of size changes in the brain and spleen, and similar but slightly earlier growth in the liver. (Figure 1B/2A, full results shown in Supplemental Data). Analyzing the 24 shrews collected for all stages of DP (large brained Summer Juvenile=5; shrinking Autumn Juvenile n=4; small brained Winter Juvenile n=5; regrowing Spring Adult n=5; regrown Summer Adult n=5), we found body mass shrank as expected between Summer Juveniles and Winter Juveniles ($BM_{WiJ-SuJ}$=-1.00g, $p_{WiJ-SuJ}$<0.028), with regrowth as they mature to Spring Adults ($BM_{SpA-WiJ}$=3.724, $p_{SpA-WiJ}$<0.0001). Shrew liver mass (Figure 1) reached a minimum as Autumn Juveniles ($LiM_{AuJ-SuJ}$=-94.1mg/g of BM, $p_{AuJ-SuJ}$=0.0949). Although regrowth began slightly early as Winter Juveniles ($LiM_{WiJ-AuJ}$=70.4/g of BM, $p_{WiJ-AuJ}$=1.0), the significant portion of regrowth still occurred between the Winter Juvenile and Spring Adult phases ($LiM_{SpA-AuJ}$=607.0mg/g of BM, $p_{SpA-WiJ}$=0.001). Brain (Figure 2) and spleen mass followed the same pattern, as Summer Juveniles reached a minimum by the Winter Juvenile phase ($BrM_{WiJ-SuJ}$=-54.4mg, $p_{WiJ-SuJ}$=0.048; $SpM_{WiJ-SuJ}$=-53.1mg/g of BM, $p_{WiJ-SuJ}$<0.001), with regrowth into Spring Adults ($BrM_{SpA-WiJ}$=71.2mg, $p_{SpA-WiJ}$=.297, $SpM_{SpA-WiJ}$=63.7mg/g of BM, $p_{SpA-WiJ}$<0.01), although not significantly in the brain. Overall, these size changes validated previous research and are further used to guide transcriptomic characterization of DP.

Reversible metabolic shifts from lipid metabolism to gluconeogenesis during shrinkage

We characterized the plasma metabolome to quantify metabolites throughout the cycle and evaluated the potential shifts in metabolism during shrinkage and regrowth. Of 250 metabolites validated by multiple detection methods in all seasons, we found 28 with significantly different concentrations varying by stage of DP (p<0.05, Figure 1A). Of these differentially concentrated metabolites, three were lipid metabolites; arachidonic acid (p=0.04), ethyl palmitoleate (p=0.02), and docosahexanoic acid (p=0.04). Compared to both Summer Juveniles and Adults, these three lipid metabolites were generally lowest in Autumn Juveniles, Winter Juveniles, and Spring Adults. This could indicate either limited lipid resource availability as size change occurs and, potentially, suppressed lipid metabolism, or lipids metabolized to generate energy are consumed faster than being generated.

To determine if changes in the metabolome were the result of the regulatory effects of gene expression on size change and suppressed lipid metabolism, we analyzed variation across five seasons and quantified differential expression of the metabolically active liver. Instead of resulting from ontogenetic or gradual changes of expression during the shrew lifespan, most of the liver differentially expressed genes (Figure 1C) fell into two temporal clusters, 8 and 12 (Figure 1D), corresponding to genes transiently up- and downregulated during the wintering cycle. Several key transcription factors (*31*, *32*) were differentially expressed mirroring liver size changes, including PPARs, CREBPs, RXRs, and FOXOs. While FOXO1 and FOXO3 promote gluconeogenesis and are reversibly upregulated in Autumn Juveniles, PPARA, PPARD, RXRA, and RXRG are both reversibly downregulated and associated with lipid metabolism (Supplemental Table 1, Figure 1E). All the mentioned liver nutrient sensing transcription factors and the genes they control are differentially expressed mirroring size changes (Supplemental Table 1), indicating large seasonal shifts in metabolism associated with brain size plasticity. We also identified a single clock gene, PER1, reversibly upregulated in Autumn Juveniles, and the upregulation of genes associated with endocrine signaling from the liver to the blood (POMC, VDR, NRG1, FGFR4, FGF21). Differentially expressed liver nutrient sensing, clock transcription factors, and endocrine genes are known to control gene expression and regulate metabolism, indicating a switch from lipid to glucose fuel during autumnal shrinkage and initial decline of circulating lipid availability. This switch parallels mechanisms implicated in evolutionary adaptations to wintering and hypoxia, as well as hypothesized metabolic dysregulation associated with neurodegeneration (*12*, *33*).

Differential expression analyses focused on genes of high effect, but large modules comprising genes with small effect could also play a pivotal role in regulating seasonal metabolic changes. We characterized interactions in expression among genes and identified modules of co-regulated liver-expressed genes related to seasonal changes in body and liver size using weighted gene co-expression network analysis (WGCNA). We identified 37 modules (Supplemental Figure 2A), of which ten are significantly associated with growth or size changes (Figure 3A). Among these, one module, cyan, encompassed 2,816 genes and correlated with all reversible body and liver size changes. Unlike other modules also significantly associated with summer controls, co-expression in the cyan module is exclusively related to size changes. Therefore, genes in the cyan module are associated with the cyclic shifts defining DP through transient activation and deactivation. In this module, we identified 76 significantly enriched pathways that together form 16 pathway clusters (Figure 3B, Supplemental Data). The most enriched of these pathway clusters comprises four pathways (Figure 3C): insulin resistance, longevity regulating pathway, AMPK signaling pathway, and longevity regulating pathway (across multiple species); and included transcription factors (PPARA, FOXO1, CREB3L2, CREB3L3), their downstream targets (G6PC), PPARG coactivators (PPARGC1A, PPARGC1B), and regulators of inflammation (HNF4A, NFKB1). Therefore, metabolic and longevity-related co-expression in the shrew is associated with these transcription factors, which are also involved in metabolic and age-related progression of neurodegeneration in model organisms.

Decreased brain cholesterol efflux, signatures of neurodegeneration, and a brain-liver axis

We evaluated the effect of metabolic shifts on the shrew brain, which may drive observed size plasticity, while also coordinating seasonal changes in metabolism. First, to disentangle markers of shrinkage from those associated with ontogeny, we compared gene expression across stages in the hippocampus, which shrinks then regrows, and the cortex, which shrinks massively, but minimally regrows. In the hippocampus, we found 266 differentially expressed genes, only 25 of which were of high effect (Figure 2C). In contrast, the cortex showed 540 differentially expressed genes, with 96 downregulated and 65 upregulated genes of high effect at the Winter Juvenile phase (Figure 2C). Temporal gene clustering analyses revealed fewer distinct clusters in the hippocampus than the liver and cortex, but, as with the liver, most differentially expressed genes are in Clusters 3 and 11, showing transient up and down regulation consistent with DP (Supplemental Figure 4). For the cortex, most of the high effect differentially expressed genes grouped in Clusters 1 and 11, with genes in Cluster 1 showing a gradual increase in expression

through the life cycle and genes in Cluster 11 being permanently downregulated between the Autumn Juvenile and Winter Juvenile periods. Despite less variation in gene expression between stages in the brain than in the liver, we identified unique brain-region-specific responses to DP and gene expression patterns consistent with both ontogenetic brain development and DP, especially in the hippocampus.

Testing for differential expression during size change in the hippocampus and cortex, we found few overlapping differentially expressed genes, but both tissue-specific gene sets were enriched for the cholesterol metabolism pathway (Figure 2D), including the apolipoproteins APOA1 and APOH (Figure 2B). In each tissue, the cholesterol metabolism pathway shows a similar trend: cholesterol metabolism upregulated during initial growth and regrowth in the hippocampus, and downregulated during cortex shrinkage, indicating this pathway's crucial role in both shrinkage and regrowth. Gene co-expression network analyses of the hippocampus also revealed 34 modules (Supplemental Figure 3), three of which correlated with brain shrinkage (Figure 4A). The most significant of these modules (grey) comprised 346 genes, and is associated with both metabolic processes and glycolysis, as well as enriched with genes —such as CASP3, PPARG, CREB3L2, CALM3— in pathways known to underlie neurodegenerative pathogenesis including pathways of neurodegeneration, Parkinson's disease, and Huntington's disease (Figure 4C). Although centered on the key glycolytic enzyme ALDOA (Figure 4B), the regulator of lipid metabolism and transcription factor PPARG is also central to this module. While gene expression patterns in the brain and the liver are distinct, both related through signals of reversible fluctuations in metabolic energy sources. Evidence of both a switch to glucose metabolism in the liver and downregulation of cholesterol metabolism in the brain during shrinkage is consistent with a nadir in circulating lipid metabolites in winter. We therefore propose that shifts in the regulation of lipids in the liver and brain, mirrored by shifting metabolite concentrations in the blood, indicate a pivotal role for regulatory coordination via a brain-liver crosstalk in DP.

Discussion

For the first time we characterized a range of molecular shifts associated with brain shrinkage and regrowth in *Sorex araneus*. Previous research suggested winter size reduction reduced energy expenditure of large and energy expensive tissue (*5*, *7*, *34*, *35*), but at a cost for the brain, which experiences architectural change and cognitive decline during shrinkage (*2*, *36*). Exploring this metabolic hypothesis, stage-by-stage analysis of blood metabolites indicates similarities to hypoxic strategies instead of hibernation, while analysis of RNA brain expression during shrinkage revealed both markers of decreased cholesterol efflux and correlations with pathways of neurodegenerative disease. These changes in brain expression occurred after the body and liver showed drastic yet reversible metabolic shifts from lipid to glucose metabolism during shrinkage and regrowth. Circadian clock genes appeared to regulate shifts in liver metabolism, along with changes in hepatokine and endocrine signals that can permeate the BBB. We therefore propose a crosstalk between the brain and liver underlies metabolic and seasonal size changes in DP, despite the protective functions of the BBB that isolate brain from body metabolism. This crosstalk between brain and liver metabolism in the healthy shrew going through its annual cycle shows parallels to mechanisms of human neurodegeneration.

If shrew metabolic shifts paralleled those in hibernation, an increase in lipid metabolites would be observed during shrinkage. Instead, we found autumn, winter, and spring reductions in arachidonic acid, ethyl palmitoleate, and docosahexanoic acid (Figure 1A). Increased concentration of these lipid metabolites has been found in hibernators that shift fuel source from carbohydrates to lipids in winter including the arctic ground squirrel (*37*), hedgehog (*38*), echidna (*39*), brown bear (*15*), and hamster (*40*, *41*). By contrast, shrew metabolite variation during winter more closely resembles conserved hypoxia responses previously found in naked mole rats (*42*), yaks (*43*), and even goldfish (*44*). In hypoxic naked mole rats, stored liver glucose is released into the blood to fuel carbohydrate metabolism (*45*), as the mole rats remain active with only slight reductions in metabolic rate (*46*). Like mole rats in their fossorial environment, semi-fossorial

shrews stay active throughout the winter. Instead of mimicking hibernation, shrew metabolites indicate a hypoxia-like shift to glucose as fuel as a lipid conservation mechanism for periods of energy deficit beginning with autumn shrinkage. We argue this metabolic shift is the foundation of the observed seasonal brain shrinkage.

While metabolomic data implicated hypoxia-like constraints on circulating lipids, how gene regulation mediated these decreases was unresolved. By analyzing seasonal differential expression of metabolically important liver transcription factors, we discovered a switch in autumn shrinkage to a new primary fuel: glucose. While lipid metabolism genes (e.g., PPARA, PPARD, RXRA, and RXRG) are downregulated, increased PER1 expression signals metabolic demands met by glucose. Indicating this switch, two forkhead box transcription factors (FOXOs) associated with glucose metabolism are significantly upregulated during autumn shrinkage (Figure 2C). In mice, FOXO1 and FOXO3 stimulate gluconeogenesis that promotes hepatic glucose production, with glucose released into the blood for energy utilization throughout the body (*47*–*49*). FOXO1 and FOXO3 also impede lipid metabolism in response to fasting glucose levels (*32*, *47*, *48*, *50*). Upregulation of these transcription factors in autumn shrews, later reversed in spring, may regulate organismal energy homeostasis by promoting glucose utilization as mobilization of stored lipids decreases during shrinkage, as in hypoxia.

FOXO upregulation maintains shrew metabolic homeostasis during challenging environmental conditions and lipid scarcity, but this incurs costs to both shrew brain size and longevity. The liver co-expression network (cyan) most associated with size change was enriched for genes involved in glucose utilization and longevity associated pathways, which encompassed both *FOXO1* and *SIRT1* (Figure 3). In model organisms including *C. elegans*, *Drosophila*, mice, and humans, FOXO1 overexpression can decrease size and extend lifespan, while inhibition leads to aging and senescence (*51*–*54*). In the shrew, extreme brain size plasticity in response to FOXO1 dependent glucose utilization reduces mortality during harsh winters but may undermine shrew longevity when reversed in spring, as a terminal investment for growth and reproduction. FOXO1 cycling could explain why compared to other mammals of similar size, *S. araneus* have high metabolic rates (*35*) and short lifespan (*55*), both extreme and disproportionate to their body size. Neurodegeneration is also considered an age-related neurological disorder. Enrichment of metabolically related- and longevity regulating genes, including *FOXO1* and *SIRT1*, in this cyan gene co-expression network further highlights interactions among metabolic shifts, size, and age-related effects. Genes in this network are therefore candidates for potential therapeutic reversals of brain size decline after the onset of symptoms.

Although metabolite and liver transcriptomics results implicated overall shrew metabolism as a regulator of size plasticity, we sought to identify both the impacts of and effects on the brain. Within the hippocampal gene networks (Figure 4), there was an enrichment of genes centered on the key glycolytic enzyme ALDOA. *ALDOA* encodes an important enzyme in glycolysis that converts dietary glucose into energy by catalyzing the conversion of fructose biphosphate into glyceraldehyde 3 phosphate (*56*, *57*). Genes in the network surrounding this hub, CASP3, PPARG, CREB3L2, and CALM3, enrich pathways of neurodegeneration, including Huntington's disease and Parkinson's disease. *ALDOA* is central in this network, indicating that glycolysis regulation and shifts in glucose metabolism during shrew brain shrinkage directly regulate previously identified human neurodegenerative markers. This result further highlights similarities in the mechanisms of both shrew brain shrinkage induced via metabolic change and human neurodegeneration.

Despite these glucose-related changes, we found the shrew's shrinking brain attempts to maintain internal lipid homeostasis by reducing cholesterol efflux, likely as neuroprotection. Changes in lipid metabolism can occur in the brain to compensate for energy deficits by self-catabolizing fats (*58*), but maintenance of metabolic homeostasis is important for neural health (*59*, *60*). Therefore, self-catabolism of the shrew brain would undermine function during the winter

months. Except for RXRG, lipid metabolism transcription factors differentially expressed in the liver during seasonal size change (PPARA, PPARB, RXRA) were *not* differentially expressed in the shrew brain. Instead, differential expression analyses indicate limits to brain cholesterol efflux during shrinkage via apolipoproteins (APOs; Figure 2). These signals suggest the shrew brain protects itself from bodily lipid constraints by limiting cholesterol efflux during lipid scarcity and high turnover in winter.

Lastly, we propose a brain-liver crosstalk regulates shifts in glucose and lipid metabolism, organ size-changes, and neuroprotective changes in brain cholesterol efflux. Although the brain communicates extrinsic environmental signals to the rest of the body, the blood brain barrier limits the relay of environmental information back to the brain. We identified several gene expression patterns associated with molecules that both cross this semi-permeable barrier and are likely involved in brain size change. As circadian clock gene PER1 is downregulated, there is upregulation of genes involved in endocrine signaling in the liver. Endocrine signaling between the brain and liver has been shown to regulate glucose homeostasis (*61*) and is promoted by circadian clock genes (*62*). Additionally, the large liver co-expression module of seasonal size change (cyan) is significantly enriched with AMPK signaling genes in (cyan, Figure 3C). Across mammals, AMPK signaling restores energy balance by transitioning between anabolic and catabolic pathways in response to circulating glucose levels through tissue-specific cross-modulation (*63*, *64*). In shrews, liver-specific change in AMPK signaling, in tandem with circadian and endocrine signaling, modulates both brain and liver expression changes in response to the transition from lipids to glucose as main fuel source.

Coordinated changes in gene expression of the liver and brain, the proposed brain-liver axis, are ideal candidate mechanisms of brain shrinkage. Functional relationships, or axes, as the brain receives stimuli from peripheral tissues can induce vast changes in brain function, expression, and phenotype. These stimuli range from inflammatory responses sent from the spleen (*65*) to regulation of nutrient metabolism through signals from the gut microbiota (*66*). In mammals, alterations to the brain-liver axis have been implicated in several models of neurodegenerative disease (*67–70*). For example, in mice models of Parkinson's disease, nigrostriatal degeneration results in hepatic mitochondrial dysfunction, causing metabolic dysregulation that self-perpetuates initial neurodegenerative symptoms (*68*). Reversals of candidate genes and pathways within this brain-liver axis, however, indicate these processes in the shrew are self-perpetuating. Instead, the reversals suggest effective self-regulation that not only drives shrinkage, but also allows brain regrowth. Expression reversals via the brain-liver axis are thus important targets for functional tests and future therapeutic treatments.

Dehnel's phenomenon was known to be an energy saving adaptation that incurred some cognitive compromise (*2*), but its molecular underpinnings were largely unknown. In shrew liver and blood plasma, we discovered shifts from lipid to sugar metabolism during shrinkage, in tandem with upregulated indicators of neurodegeneration in the brain. But in contrast with mammalian models for neurodegenerative diseases, the shrew brain also enters a state of fat conservation by seemingly limiting cholesterol efflux in the winter, the most metabolically demanding phase of the shrew's brief life. Based on our results, we propose this combination of sugar-dependent whole-body metabolism and limited brain cholesterol efflux is an evolved form of neuroprotection within the constraints of the shrew's environment and life history. Our study thus sheds light on relationships between metabolic regulation and neurodegenerative disease, with implications for therapeutic medical research.

Materials and Methods

Further details of experimental protocols are described in SI Appendix. Code and data can be found on GitHub: https://github.com/wrthomas315/Dehnels_Seasonal_RNAseq/tree/main/data

Sample Collection and RNA Sequencing

Eurasian common shrews were trapped with insulated wooden traps in Radolfzell, Germany, at five different stages of development: large-brained Summer Juveniles (n=5), shrinking Autumn Juveniles (n=4), small brained Winter Juveniles (n=5), regrowing Spring Adults (n=5), and regrown Summer Adults (n=5) (Supplemental Table 1). Shrews were aged and sexed based on tooth wear, fur appearance, and gonad development prior to euthanasia. Fewer females than males were sampled in juvenile stages (n=6 females), this has minimal effect on gene expression as shrews are prepubescent and not sexually dimorphic at that age. Only minor sex dimorphism was detected in the size change of representative brain regions in a previous study (*2*). Blood was collected prior to perfusion through the heart, let stand for 15 minutes, spun down at 1200 rpm, the serum pipetted off and then stored at -80°C. Shrews were perfused under anesthesia via the vascular system with PAXgene Tissue Fixative. All organs were removed and weighed to confirm the occurrence of DP. Thoracic organs were then placed immediately into PAXgene Tissue Stabilizer, while the brain was submerged in cold fixative, dissected into each region, and then placed into PAXgene Tissue Stabilizer. All samples were placed in stabilizer (2-24 hours after extraction) and then stored in liquid nitrogen. RNA was extracted with a modified Qiagen Micro RNAeasy protocol used for small amounts of mammalian sensory tissue. Tissues extracted included the liver, cortex, and hippocampus. The hippocampus and cortex were chosen, as they both undergo substantial non sex-biased shrinkage (*2*), while also the regions most affected by neurovegetative diseases such as Alzheimer's disease (*71*). Therefore, these may be the most informative for future therapeutic purposes. RNA was sent to Genewiz for quality control, library preparation, and sequencing. Quantity of RNA was measured with a Nanodrop spectrophotometer and quality of RNA assessed with RNA ScreenTape. Libraries were prepared with standard polyA selection and sequenced as 150bp pair-end reads for a target of 15-25 million reads per sample. To confirm the occurrence of DP, thoracic organs were normalized by body weight and tested for significant change in mean normalized mass using a t-test between stages. For the brain, mass was not normalized as change in size itself is of interest, regardless of parallel changes in body mass.

Temporal Clustering Differential Gene Expression Analysis

We trimmed adapters and filtered reads using fastp (*72*) and removed samples with extreme read counts (~10-fold). Gene counts were quantified by pseudo aligning to the 19,296 protein coding genes of the *S. araneus* genome (sorAra2; GCF_000181275.1) using Kallisto (*73*). Counts were normalized for each tissue using DESeq2 (*74*) median of ratios. We used these normalized gene expressions to also analyze gene expression through time using the package TCseq (*75*). To remove genes with relatively little change in expression, we filtered each organ set for genes with an absolute fold change less than 0.5 between any two stages. Next, we filtered any gene with extremely low expression, such that two samples had to have greater than ten normalized reads. We then transformed each gene expression profile across stages to z-scores, and then used fuzzy cmeans clustering to identify clusters of similar gene expression profiles. The number of resultant gene clusters was found by bootstrapping (n=20) a gap statistic that minimized the within-cluster distance (standard error from center). Seasonal cluster membership was compared to high-effect significant results from differential gene expression analyses below.

Differential Gene Expression Analysis

Tests for differential gene expression were conducted between the phenotypically extreme stages of the same tissue. For the liver, Autumn Juveniles and Spring Adults were compared, which also overlap with the spleen, hippocampus, and cortex shrinking and regrowth phases, such that we could make inferences about potential extrahepatic signals. Winter Juveniles (hippocampus minimum) and Spring Adults (hippocampus regrowth) were compared. For the cortex, Summer Juveniles (before shrinkage) and Winter Juveniles (cortex minimum) were compared, as the cortex does not enter a period of substantial regrowth (*2*). Normalized counts for each gene was fitted with a negative binomial generalized linear model and then we used a Wald test to examine if differences in gene expression was the result of the season parameter, with p-values corrected

using the Benjamini and Hochberg procedure (*76*). We filtered our significant results for significant genes higher and lower than 1.58 log-fold change (absolute 3-fold change), to identify how many significant differentially expressed genes were of high effect, largely for gene set enrichments, thus reducing the number of resultant genes to improve interpretability. The hippocampus data had very few differentially expressed genes when filtered (n=25), thus, log-fold change filtering was omitted for this tissue. We then identified enriched KEGG Gene Ontology (GO) pathways in the gene data sets using DAVID functional annotation (*77*).

Weighted Gene Co-expression Network Analysis

We used the WGCNA package (*78*) package to create co-expression networks for the liver and hippocampus and determined if these correlations between genes are significantly correlated with our shrinkage and regrowth phenotypes. Network construction parameters and code can be found in the SI Appendix and on GitHub. Cytoscape (*79*) was used to visualize significant networks and calculate network statistics such as node (gene) connectivity. Identification of potential function of each module were analyzed using DAVID Gene Functional Classification Tool to test for GO enrichment (*77*).

Metabolomics

Metabolite analysis was carried out by MS-Omics using a Thermo Scientific Vanquish LC (UPLC) coupled to Thermo Q Exactive HF MS. Identification of compounds were performed at four levels; Level 1: identification by retention times (compared against in-house authentic standards), accurate mass (with an accepted deviation of 3ppm), and MS/MS spectra, Level 2a: identification by retention times (compared against in-house authentic standards), accurate mass (with an accepted deviation of 3ppm). Level 2b: identification by accurate mass (with an accepted deviation of 3ppm), and MS/MS spectra. MetaboAnalyst was used to test for changes in concentration between seasons (*80*). Concentrations for each sample were normalized by the average concentration of our Summer Adults samples and log transformed and auto scaled. A one-way ANOVA was used to test for any significant seasonal difference in metabolite concentration, with p-values corrected with a false discovery rate of 0.05. Within each significant metabolite, t-tests were used to identify pairwise differences in mean between each season. Samples were hierarchically clustered using significant genes and visualized using a heatmap.

Acknowledgments

We thank Joshua Rest, Krishna Veeramah, and Tanya Lama who have provided helpful feedback on initial results and previous versions of the manuscript. We thank Michal Oklinski for help with initial dissections.

Funding

WRT and research were supported by the Human Frontiers in Science Program Award (RGP0013/2019) to DD, LMD, and JN, and by the Stony Brook University Presidential Innovation and Excellence Fund to LMD.

References

1. Z. Pucek, Seasonal and age changes in the weight of internal organs of shrews. *Acta Theriol. (Warsz).* **10**, 369–438 (1965). doi:10.4098/at.arch.65-31.
2. J. Lázaro, M. Hertel, C. C. Sherwood, M. Muturi, D. K. N. Dechmann, Profound seasonal changes in brain size and architecture in the common shrew. *Brain Struct. Funct.* **223**, 2823–2840 (2018). doi:10.1007/s00429-018-1666-5. http://dx.doi.org/10.1007/s00429-018-1666-5.
3. S. Ray, M. Li, S. P. Koch, S. Mueller, P. Boehm-Sturm, H. Wang, M. Brecht, R. K. Naumann, Seasonal plasticity in the adult somatosensory cortex. *Proc. Natl. Acad. Sci. U. S. A.* **117**, 32136–32144 (2020). doi:10.1073/pnas.1922888117.
4. M. Genoud, K. Isler, R. D. Martin, Comparative analyses of basal rate of metabolism in mammals : data selection does matter. *Biol. Rev.* **93**, 404–438 (2018).

doi:10.1111/brv.12350.

5. L. Keicher, M. T. O'Mara, C. C. Voigt, D. K. N. Dechmann, Stable carbon isotopes in breath reveal fast metabolic incorporation rates and seasonally variable but rapid fat turnover in the common shrew (Sorex araneus). *J. Exp. Biol.* **220**, 2834–2841 (2017). doi:10.1242/jeb.159947.
6. H. Hyvärinen, Wintering strategy of voles and shrews in Findland. *Winter Ecol. Small Mamm.* **10**, 139–148 (1984).
7. P. J. Schaeffer, M. T. O'Mara, J. Breiholz, L. Keicher, J. Lázaro, M. Muturi, D. K. N. Dechmann, Metabolic rate in common shrews is unaffected by temperature, leading to lower energetic costs through seasonal size reduction. *R. Soc. Open Sci.* **7** (2020). doi:10.1098/rsos.191989.
8. J. Lázaro, M. Hertel, M. Muturi, D. K. N. Dechmann, Seasonal reversible size changes in the braincase and mass of common shrews are flexibly modified by environmental conditions. *Sci. Rep.* **9**, 1–10 (2019). doi:10.1038/s41598-019-38884-1.
9. P. Mergenthaler, U. Lindauer, G. A. Dienel, A. Meisel, Sugar for the brain: The role of glucose in physiological and pathological brain function. *Trends Neurosci.* **36**, 587–597 (2013). doi:10.1016/j.tins.2013.07.001.
10. D. A. Elliott, C. S. Weickert, B. Garner, Apolipoproteins in the brain: Implications for neurological and psychiatric disorders. *Clin. Lipidol.* **5**, 555–573 (2010). doi:10.2217/clp.10.37.
11. R. Agrawal, F. Gomez-Pinilla, "Metabolic syndrome" in the brain: Deficiency in omega-3 fatty acid exacerbates dysfunctions in insulin receptor signalling and cognition. *J. Physiol.* **590**, 2485–2499 (2012). doi:10.1113/jphysiol.2012.230078.
12. C. Sims-Robinson, B. Kim, A. Rosko, E. L. Feldman, How does diabetes accelerate Alzheimer disease pathology? *Nat. Rev. Neurol.* **6**, 551–559 (2010). doi:10.1038/nrneurol.2010.130.
13. H. Macpherson, M. Formica, E. Harris, R. M. Daly, Brain functional alterations in Type 2 Diabetes – A systematic review of fMRI studies. *Front. Neuroendocrinol.* **47**, 34–46 (2017). doi:10.1016/j.yfrne.2017.07.001. http://dx.doi.org/10.1016/j.yfrne.2017.07.001.
14. B. B. Boyer, B. M. Barnes, Molecular and metabolic aspects of mammalian hibernation. *Bioscience* **49**, 713–724 (1999). doi:10.2307/1313595.
15. B. Chazarin, K. B. Storey, A. Ziemianin, S. Chanon, M. Plumel, I. Chery, C. Durand, A. L. Evans, J. M. Arnemo, A. Zedrosser, J. E. Swenson, G. Gauquelin-Koch, C. Simon, S. Blanc, E. Lefai, F. Bertile, Metabolic reprogramming involving glycolysis in the hibernating brown bear skeletal muscle. *Front. Zool.* **16**, 1–21 (2019). doi:10.1186/s12983-019-0312-2.
16. J. L. Villanueva-Cañas, S. L. Faherty, A. D. Yoder, M. M. Albà, Comparative genomics of mammalian hibernators using gene networks. *Integr. Comp. Biol.* **54**, 452–462 (2014). doi:10.1093/icb/icu048.
17. S. L. Faherty, J. Luis Villanueva-Cañas, P. H. Klopfer, M. M. Albà, A. D. Yoder, Gene expression profiling in the hibernating primate, Cheirogaleus medius. *Genome Biol. Evol.* **8**, 2413–2426 (2016). doi:10.1093/gbe/evw163.
18. P. W. Hochachka, Defense Strategies against Hypoxia and Hypothermia. *Science (80-.).* **231**, 234–241 (1986).
19. K. L. Drew, M. E. Rice, T. B. Kuhn, M. A. Smith, Neuroprotective adaptations in hibernation: Therapeutic implications for ischemia-reperfusion, traumatic brain injury and neurodegenerative diseases. *Free Radic. Biol. Med.* **31**, 563–573 (2001). doi:10.1016/S0891-5849(01)00628-1.
20. K. R. Dave, S. L. Christian, M. A. Perez-Pinzon, K. L. Drew, Neuroprotection: Lessons from hibernators. *Comp. Biochem. Physiol. - B Biochem. Mol. Biol.* **162**, 1–9 (2012). doi:10.1016/j.cbpb.2012.01.008.
21. A. P. Ross, S. L. Christian, H. W. Zhao, K. L. Drew, Persistent tolerance to oxygen and nutrient deprivation and N-methyl-D-aspartate in cultured hippocampal slices from hibernating Arctic ground squirrel. *J. Cereb. Blood Flow Metab.* **26**, 1148–1156 (2006).

519 doi:10.1038/sj.jcbfm.9600271.
520 22. J. A. Davis, J. R. Paul, L. J. McMeekin, S. R. Nason, J. P. Antipenko, S. D. Yates, R. M.
521 Cowell, K. M. Habegger, K. L. Gamble, High-Fat and High-Sucrose Diets Impair Time-of-
522 Day Differences in Spatial Working Memory of Male Mice. *Obesity* **28**, 2347–2356 (2020).
523 doi:10.1002/oby.22983.
524 23. A. Jayaraman, D. Lent-Schochet, C. J. Pike, Diet-induced obesity and low testosterone
525 increase neuroinflammation and impair neural function. *J. Neuroinflammation* **11**, 1–14
526 (2014). doi:10.1186/s12974-014-0162-y.
527 24. M. P. Mattson, T. V. Arumugam, Hallmarks of Brain Aging: Adaptive and Pathological
528 Modification by Metabolic States. *Cell Metab.* **27**, 1176–1199 (2018).
529 doi:10.1016/j.cmet.2018.05.011. https://doi.org/10.1016/j.cmet.2018.05.011.
530 25. T. S. Reese, M. J. Karnovsky, Fine structural localization of a blood-brain barrier to
531 exogenous peroxidase. *J. Cell Biol.* **34**, 207–217 (1967). doi:10.1083/jcb.34.1.207.
532 26. G. A. Rosenberg, Neurological diseases in relation to the blood-brain barrier. *J. Cereb.*
533 *Blood Flow Metab.* **32**, 1139–1151 (2012). doi:10.1038/jcbfm.2011.197.
534 http://dx.doi.org/10.1038/jcbfm.2011.197.
535 27. B. D. Zipser, C. E. Johanson, L. Gonzalez, T. M. Berzin, R. Tavares, C. M. Hulette, M. P.
536 Vitek, V. Hovanesian, E. G. Stopa, Microvascular injury and blood-brain barrier leakage in
537 Alzheimer's disease. *Neurobiol. Aging* **28**, 977–986 (2007).
538 doi:10.1016/j.neurobiolaging.2006.05.016.
539 28. B. V. Zlokovic, Neurovascular pathways to neurodegeneration in Alzheimer's disease and
540 other disorders. *Nat. Rev. Neurosci.* **12**, 723–738 (2011). doi:10.1038/nrn3114.
541 29. A. D. Wong, M. Ye, A. F. Levy, J. D. Rothstein, D. E. Bergles, P. C. Searson, The blood-
542 brain barrier: An engineering perspective. *Front. Neuroeng.* **6**, 1–22 (2013).
543 doi:10.3389/fneng.2013.00007.
544 30. D. Wang, J. M. Pascual, H. Yang, K. Engelstad, X. Mao, J. Cheng, J. Yoo, J. L. Noebels,
545 D. C. De Vivo, A mouse model for Glut-1 haploinsufficiency. *Hum. Mol. Genet.* **15**, 1169–
546 1179 (2006). doi:10.1093/hmg/ddl032.
547 31. P. Nguyen, V. Leray, M. Diez, S. Serisier, J. Le Bloc'H, B. Siliart, H. Dumon, Liver lipid
548 metabolism. *J. Anim. Physiol. Anim. Nutr. (Berl).* **92**, 272–283 (2008). doi:10.1111/j.1439-
549 0396.2007.00752.x.
550 32. Z. Yang, K. Roth, M. Agarwal, W. Liu, M. C. Petriello, The transcription factors CREBH,
551 PPARa, and FOXO1 as critical hepatic mediators of diet-induced metabolic dysregulation.
552 *J. Nutr. Biochem.* **95**, 108633 (2021). doi:10.1016/j.jnutbio.2021.108633.
553 https://doi.org/10.1016/j.jnutbio.2021.108633.
554 33. A. P. Corthals, Multiple sclerosis is not a disease of the immune system. *Q. Rev. Biol.* **86**,
555 287–321 (2011). doi:10.1086/662453.
556 34. Z. Pucek, Seasonal and age change in shrews as an adaptive process. *Symp. zool. Soc.*
557 *Lond.* **26**, 189–207 (1970).
558 35. J. R. E. Taylor, Evolution of Energetic Strategies in Shrews. *Evol. Shrews*, 309–346
559 (1998).
560 36. J. Lázaro, M. Hertel, S. LaPoint, M. Wikelski, M. Stiehler, D. K. N. Dechmann, Cognitive
561 skills of common shrews (Sorex araneus) vary with seasonal changes in skull size and
562 brain mass. *J. Exp. Biol.* **221**, 1–6 (2018). doi:10.1242/jeb.166595.
563 37. S. A. Rice, M. Mikes, D. Bibus, E. Berdyshev, J. A. Reisz, S. Gehrke, I. Bronova, A.
564 D'Alessandro, K. L. Drew, Omega 3 fatty acids stimulate thermogenesis during torpor in
565 the Arctic Ground Squirrel. *Sci. Rep.* **11**, 1–14 (2021). doi:10.1038/s41598-020-78763-8.
566 https://doi.org/10.1038/s41598-020-78763-8.
567 38. S. Laukola, Seasonal changes in the fatty acid spectrum of the hedgehog's white and
568 brown adipose tissue. *Ann. Zool. Fennici* **17**, 191–201 (1980).
569 39. F. Falkenstein, G. Körtner, K. Watson, F. Geiser, Dietary fats and body lipid composition
570 in relation to hibernation in free-ranging echidnas. *J. Comp. Physiol. - B Biochem. Syst.*
571 *Environ. Physiol.* **171**, 189–194 (2001). doi:10.1007/s003600000157.
572 40. S. Giroud, C. Frare, A. Strijkstra, A. Boerema, W. Arnold, T. Ruf, Membrane Phospholipid

Fatty Acid Composition Regulates Cardiac SERCA Activity in a Hibernator, the Syrian Hamster (Mesocricetus auratus). *PLoS One* **8** (2013). doi:10.1371/journal.pone.0063111.

41. F. Geiser, M. Klingenspor, B. M. McAllan, A Functional Nexus between Photoperiod Acclimation, Torpor Expression and Somatic Fatty Acid Composition in a Heterothermic Mammal. *PLoS One* **8** (2013). doi:10.1371/journal.pone.0063803.
42. M. R. Pergande, V. G. Amoroso, T. T. A. Nguyen, W. Li, E. Vice, T. J. Park, S. M. Cologna, PPARα and PPARγSignaling Is Enhanced in the Brain of the Naked Mole-Rat, a Mammal that Shows Intrinsic Neuroprotection from Oxygen Deprivation. *J. Proteome Res.* **20**, 4258–4271 (2021). doi:10.1021/acs.jproteome.1c00131.
43. X. Meng, J. Zhou, J. Li, R. Wan, H. Yu, Q. Wei, UPLC-QTOF/MS-based metabolomic analysis of plasma reveals altitude effects on yaks (Bos grunniens). *Thai J. Vet. Med.* **51**, 551–559 (2021). doi:10.14456/tjvm.2021.66.
44. E. Farhat, E. D. Turenne, K. Choi, J. M. Weber, Hypoxia-induced remodelling of goldfish membranes. *Comp. Biochem. Physiol. Part B* **237**, 1–8 (2019). doi:10.1016/j.cbpb.2019.110326. https://doi.org/10.1016/j.cbpb.2019.110326.
45. M. E. Pamenter, Adaptations to a hypoxic lifestyle in naked mole-rats. *J. Exp. Biol.* **225** (2022). doi:10.1242/jeb.196725.
46. A. M. Kirby, G. D. Fairman, M. E. Pamenter, Atypical behavioural, metabolic and thermoregulatory responses to hypoxia in the naked mole rat (Heterocephalus glaber). *J. Zool.* **305**, 106–115 (2018). doi:10.1111/jzo.12542.
47. W. Zhang, S. Patil, B. Chauhan, S. Guo, D. R. Powell, J. Le, A. Klotsas, R. Matika, X. Xiao, R. Franks, K. A. Heidenreich, M. P. Sajan, R. V. Farese, D. B. Stolz, P. Tso, S. H. Koo, M. Montminy, T. G. Unterman, FoxO1 regulates multiple metabolic pathways in the liver effects on gluconeogenic, glycolytic, and lipogenic gene expression. *J. Biol. Chem.* **281**, 10105–10117 (2006). doi:10.1074/jbc.M600272200. http://dx.doi.org/10.1074/jbc.M600272200.
48. X. Xiong, R. Tao, R. A. DePinho, X. C. Dong, Deletion of Hepatic FoxO1/3/4 Genes in Mice Significantly Impacts on Glucose Metabolism through Downregulation of Gluconeogenesis and Upregulation of Glycolysis. *PLoS One* **8**, 1–11 (2013). doi:10.1371/journal.pone.0074340.
49. M. Matsumoto, A. Pocai, L. Rossetti, R. A. DePinho, D. Accili, Impaired Regulation of Hepatic Glucose Production in Mice Lacking the Forkhead Transcription Factor Foxo1 in Liver. *Cell Metab.* **6**, 208–216 (2007). doi:10.1016/j.cmet.2007.08.006.
50. I. Tikhanovich, J. Cox, S. A. Weinman, Forkhead box class O transcription factors in liver function and disease. *J. Gastroenterol. Hepatol.* **28**, 125–131 (2013). doi:10.1111/jgh.12021.
51. M. S. Gami, C. A. Wolkow, Studies of Caenorhabditis elegans DAF-2/insulin signaling reveal targets for pharmacological manipulation of lifespan. *Aging Cell* **5**, 31–37 (2006). doi:10.1111/j.1474-9726.2006.00188.x.
52. D. S. Hwangbo, B. Garsham, M. P. Tu, M. Palmer, M. Tatar, Drosophila dFOXO controls lifespan and regulates insulin signalling in brain and fat body. *Nature* **429**, 562–566 (2004). doi:10.1038/nature02549.
53. A. Satoh, C. S. Brace, N. Rensing, P. Cliften, D. F. Wozniak, E. D. Herzog, K. A. Yamada, S. I. Imai, Sirt1 extends life span and delays aging in mice through the regulation of Nk2 Homeobox 1 in the DMH and LH. *Cell Metab.* **18**, 416–430 (2013). doi:10.1016/j.cmet.2013.07.013. http://dx.doi.org/10.1016/j.cmet.2013.07.013.
54. M. Katic, C. R. Kahn, The role of insulin and IGF-1 signaling in longevity. *Cell. Mol. Life Sci.* **62**, 320–343 (2005). doi:10.1007/s00018-004-4297-y.
55. K. Healy, T. Guillerme, S. Finlay, A. Kane, S. B. A. Kelly, D. McClean, D. J. Kelly, I. Donohue, A. L. Jackson, N. Cooper, Ecology and mode-of-life explain lifespan variation in birds and mammals. *Proc. R. Soc. B Biol. Sci.* **281** (2014). doi:10.1098/rspb.2014.0298.
56. S. Du, Z. Guan, L. Hao, Y. Song, L. Wang, L. Gong, L. Liu, X. Qi, Z. Hou, S. Shao, Fructose-bisphosphate aldolase a is a potential metastasis-associated marker of lung squamous cell carcinoma and promotes lung cell tumorigenesis and migration. *PLoS One*

9 (2014). doi:10.1371/journal.pone.0085804.

57. J. H. T. Potter, R. Drinkwater, K. T. J. Davies, N. Nesi, M. C. W. Lim, L. R. Yohe, H. Chi, X. Zhang, I. Levantis, B. K. Lim, C. C. Witt, G. Tsagkogeorga, M. dos Reis, Y. Liu, W. Furey, M. J. Whitley, D. Aksentijevic, L. M. Dávalos, S. J. Rossiter, Nectar-feeding bats and birds show parallel molecular adaptations in sugar metabolism enzymes. *Curr. Biol.* **31**, 1–8 (2021). doi:10.1016/j.cub.2021.08.018.
58. C. N. Brocker, D. P. Patel, T. J. Velenosi, D. Kim, T. Yan, J. Yue, G. Li, K. W. Krausz, F. J. Gonzalez, Extrahepatic PPAR modulates fatty acid oxidation and attenuates fasting-induced hepatosteatosis in mice. *J. Lipid Res.* **59**, 2140–2152 (2018). doi:10.1194/jlr.M088419. http://dx.doi.org/10.1194/jlr.M088419.
59. D. Val-Laillet, S. Layec, S. Guérin, P. Meurice, C. H. Malbert, Changes in brain activity after a diet-induced obesity. *Obesity* **19**, 749–756 (2011). doi:10.1038/oby.2010.292. http://dx.doi.org/10.1038/oby.2010.292/nature06264.
60. R. Agrawal, Y. Zhuang, B. P. Cummings, K. L. Stanhope, J. L. Graham, P. J. Havel, F. Gomez-Pinilla, Deterioration of plasticity and metabolic homeostasis in the brain of the UCD-T2DM rat model of naturally occurring type-2 diabetes. *Biochim. Biophys. Acta - Mol. Basis Dis.* **1842**, 1313–1323 (2014). doi:10.1016/j.bbadis.2014.05.007. http://dx.doi.org/10.1016/j.bbadis.2014.05.007.
61. A. Kalsbeek, E. Foppen, I. Schalij, C. Van Heijningen, J. van der Vliet, E. Fliers, R. M. Buijs, Circadian control of the daily plasma glucose rhythm: An interplay of GABA and glutamate. *PLoS One* **3** (2008). doi:10.1371/journal.pone.0003194.
62. F. Gachon, U. Loizides-Mangold, V. Petrenko, C. Dibner, Glucose homeostasis: Regulation by peripheral circadian clocks in rodents and humans. *Endocrinology* **158**, 1074–1084 (2017). doi:10.1210/en.2017-00218.
63. S.-C. Lin, D. G. Hardie, AMPK: Sensing Glucose as well as Cellular Energy Status. *Cell Metab.* **27**, 299–313 (2018). doi:10.1016/j.cmet.2017.10.009. https://doi.org/10.1016/j.cmet.2017.10.009.
64. Y. Minokoshi, T. Alquier, H. Furukawa, Y. B. Kim, A. Lee, B. Xue, J. Mu, F. Foufelle, P. Ferré, M. J. Birnbaum, B. J. Stuck, B. B. Kahn, AMP-kinase regulates food intake by responding to hormonal and nutrient signals in the hypothalamus. *Nature* **428**, 569–574 (2004). doi:10.1038/nature02440.
65. B. Zhang, J. Zhong, Z. Gao, A Brain-Spleen Axis Regulates Humoral Immunity. *Neurosci. Bull.* **37**, 427–429 (2021). doi:10.1007/s12264-020-00610-7. https://doi.org/10.1007/s12264-020-00610-7.
66. S. Z. Wang, Y. J. Yu, K. Adeli, Role of gut microbiota in neuroendocrine regulation of carbohydrate and lipid metabolism via the microbiota-gut-brain-liver axis. *Microorganisms* **8**, 8–10 (2020). doi:10.3390/microorganisms8040527.
67. N. Zeltser, I. Meyer, G. V. Hernandez, M. J. Trahan, R. K. Fanter, M. Abo-Ismail, H. Glanz, C. R. Strand, D. G. Burrin, M. R. la Frano, R. Manjarín, M. Maj, Neurodegeneration in juvenile Iberian pigs with diet-induced nonalcoholic fatty liver disease. *Am. J. Physiol. - Endocrinol. Metab.* **319**, E592–E606 (2020). doi:10.1152/AJPENDO.00120.2020.
68. M. Vairetti, A. Ferrigno, V. Rizzo, G. Ambrosi, A. Bianchi, P. Richelmi, F. Blandini, M. T. Armentero, Impaired hepatic function and central dopaminergic denervation in a rodent model of Parkinson's disease: A self-perpetuating crosstalk? *Biochim. Biophys. Acta - Mol. Basis Dis.* **1822**, 176–184 (2012). doi:10.1016/j.bbadis.2011.11.008. http://dx.doi.org/10.1016/j.bbadis.2011.11.008.
69. Z. Huang, H. W. Lin, Q. Zhang, X. Zong, Targeting Alzheimer's Disease: The Critical Crosstalk between the Liver and Brain. *Nutrients* **14** (2022). doi:10.3390/nu14204298.
70. M. Trapecar, E. Wogram, D. Svoboda, C. Communal, A. Omer, T. Lungjangwa, P. Sphabmixay, J. Velazquez, K. Schneider, C. W. Wright, S. Mildrum, A. Hendricks, S. Levine, J. Muffat, M. J. Lee, D. A. Lauffenburger, D. Trumper, R. Jaenisch, L. G. Griffith, Human physiomimetic model integrating microphysiological systems of the gut, liver, and brain for studies of neurodegenerative diseases. *Sci. Adv.* **7** (2021). doi:10.1126/SCIADV.ABD1707.

71. X. Wang, M. L. Michaelis, E. K. Michaelis, Functional Genomics of Brain Aging and Alzheimers Disease: Focus on Selective Neuronal Vulnerability. *Curr. Genomics* **11**, 618–633 (2010). doi:10.2174/138920210793360943.
72. S. Chen, Y. Zhou, Y. Chen, J. Gu, Fastp: An ultra-fast all-in-one FASTQ preprocessor. *Bioinformatics* **34**, i884–i890 (2018). doi:10.1093/bioinformatics/bty560.
73. N. L. Bray, H. Pimentel, P. Melsted, L. Pachter, Near-optimal probabilistic RNA-seq quantification. *Nat. Biotechnol.* **34**, 525–527 (2016). doi:10.1038/nbt.3519.
74. M. I. Love, W. Huber, S. Anders, Moderated estimation of fold change and dispersion for RNA-seq data with DESeq2. *Genome Biol.* **15**, 1–21 (2014). doi:10.1186/s13059-014-0550-8.
75. L. G. Mengjun, TCseq: Time course sequencing data analysis. R package version 1.8.0. 1–8 (2019).
76. Y. Benjamini, Y. Hochberg, Controlling the False Discovery Rate : A Practical and Powerful Approach to Multiple Testing. *J. R. Stat. Soc.* **57**, 289–300 (1995).
77. D. W. Huang, B. T. Sherman, R. A. Lempicki, Systematic and integrative analysis of large gene lists using DAVID bioinformatics resources. *Nat. Protoc.* **4**, 44–57 (2009). doi:10.1038/nprot.2008.211.
78. P. Langfelder, S. Horvath, WGCNA: An R package for weighted correlation network analysis. *BMC Bioinformatics* **9** (2008). doi:10.1186/1471-2105-9-559.
79. P. Shannon, A. Markiel, O. Ozier, S. B. Nitin, J. T. Wang, D. Ramage, N. Amin, B. Schwikowski, T. Ideker, Cytoscape: A Software Environment for Integrated Models. *Genome Res.* **13**, 2498–2504 (2003). doi:10.1101/gr.1239303.metabolite. http://ci.nii.ac.jp/naid/110001910481/.
80. Z. Pang, J. Chong, G. Zhou, D. A. De Lima Morais, L. Chang, M. Barrette, C. Gauthier, P. É. Jacques, S. Li, J. Xia, MetaboAnalyst 5.0: Narrowing the gap between raw spectra and functional insights. *Nucleic Acids Res.* **49**, 388–396 (2021). doi:10.1093/nar/gkab382.

Figures

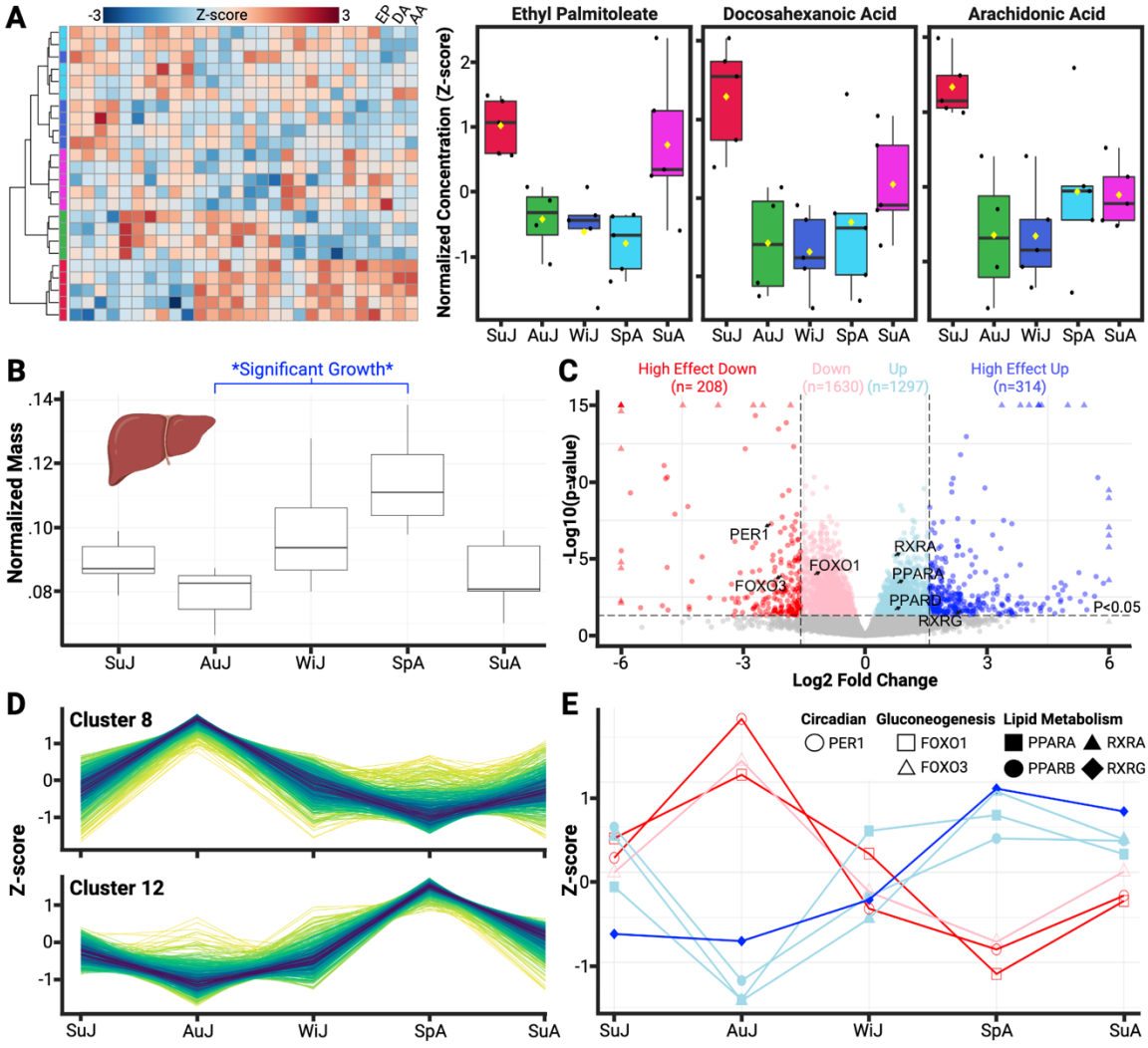

Figure 1. Metabolic profiling of the blood metabolome and liver transcriptomes. (**A)** Heatmap of 28 statistically significant differentially concentrated metabolites between stages of Dehnel's phenomenon. Hierarchical clustering using these significant metabolites groups each profile into each season. Three of these metabolites were lipid metabolites (ethyl palmitoleate, docosahexanoic acid, arachidonic acid), with decreases in autumn, winter, and spring individuals. **(B)** Mass change in liver through five stages of Dehnel's phenomenon. Unlike other organs, the liver reaches a minimum as an Autumn Juvenile, with regrowth beginning as a Winter Juvenile. Asterisks represent significant size changes (adjusted $p<0.05$). **(C)** Volcano plot of significant (adjusted $p<0.05$) differentially expressed genes (colored) between phenotypic extremes of liver size change (Spring Adult vs Autumn Juvenile) plotted by log fold-change. Vertical thresholds represent a 1.58 log fold-change in differential expression of high effect between stages (dark colors). **(D)** Temporal gene expression clusters 8 (n=95 significant genes) and 12 (n=79 significant genes), with the most significant differentially expressed genes. **(E)** Patterning of gene expression across stages of Dehnel's phenomenon for transcription factors pivotal roles in lipid metabolism and gluconeogenesis. Lipid metabolism and gluconeogenesis appear to have inverse cycles, with lipid metabolism decreasing in the fall and increasing in the spring, with gluconeogenesis following the opposite trend.

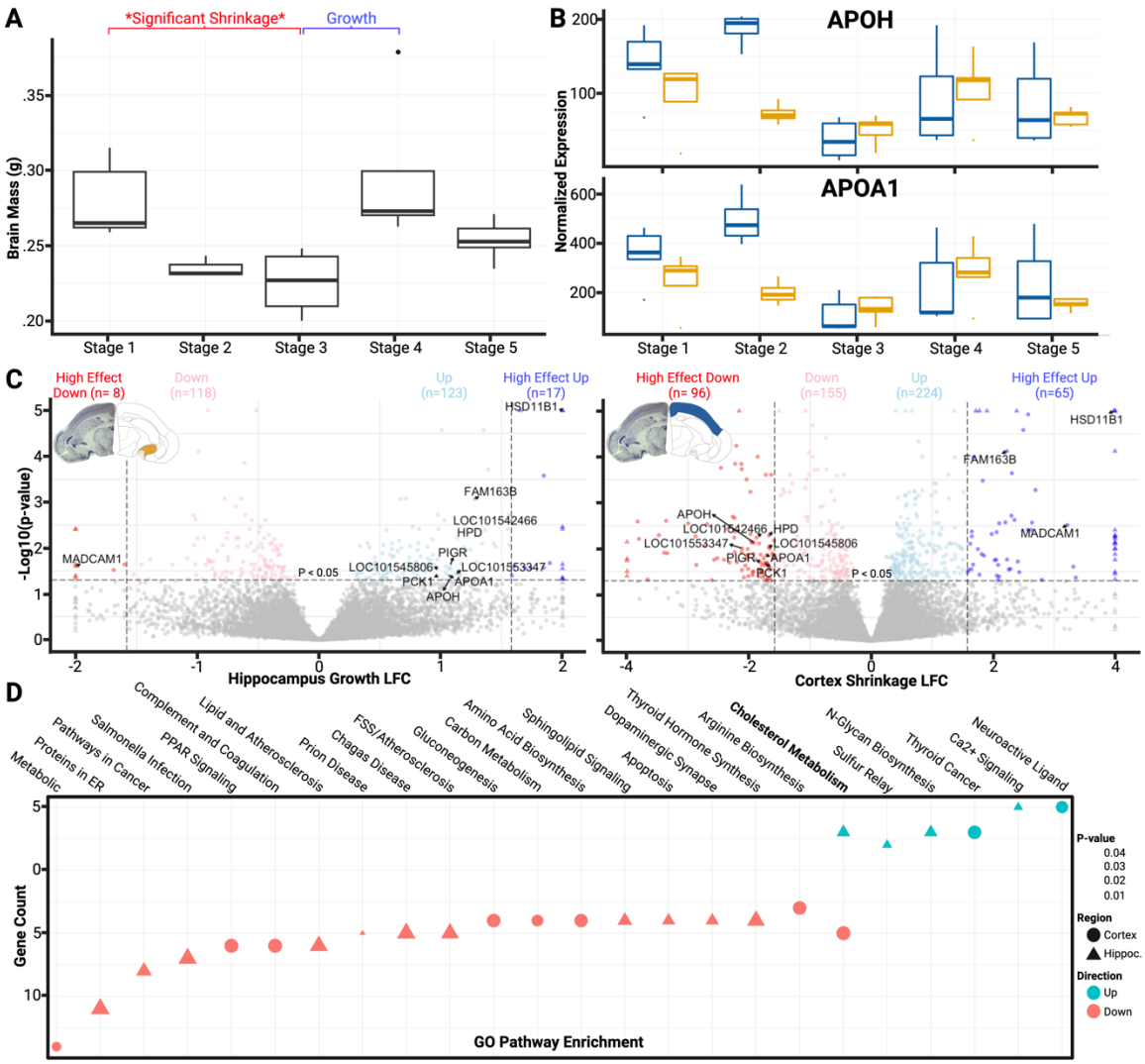

Figure 2. Seasonal plasticity in brain phenotype and expression patterns. **(A)** Brain mass change through five stages of Dehnel's phenomenon. As does body mass, the brain begins to shrink as Autumn Juveniles, reaching a minimum as Winter Juveniles, and regrows as Spring Adults. Asterisks represent significant size changes (adjusted p<0.05). **(B)** 11 genes were differentially expressed in both brain regions, including the apolipoproteins APOA1 and APOH, which both show winter decreases followed by slight spring upregulation. **(C)** Volcano plot of significant (adjusted p<0.05) differentially expressed genes (colored) in *hippocampal regrowth* (Spring Adults vs Winter Juveniles) and *cortex shrinkage* (Winter Juveniles vs Summer Juveniles) plotted by log fold-change. Vertical thresholds represent a 1.58 log fold-change which show differential expression of high effect between stages. **(D)** APOA1 and APOH are found in the cholesterol metabolism pathway, which was enriched for differentially expressed genes in both shrinkage and regrowth phenotypes.

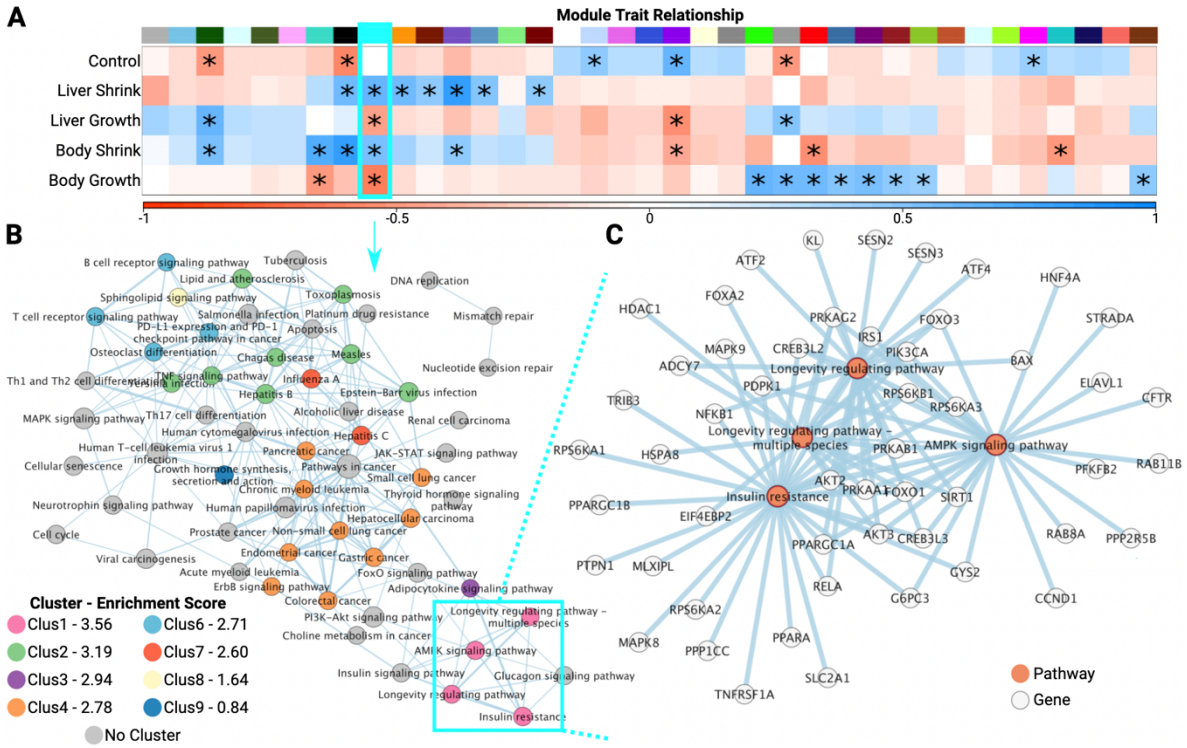

Figure 3. Gene network analyses across liver and body phenotypes of Dehnel's phenomenon. (**A**) Modules (n=37) of high gene co-expression in the liver, including 21 modules with significant correlation with at least one change phenotype (Controls, Liver Shrinkage, Liver Growth, Body Shrinkage, and Body Growth). The 2816 gene cyan module was significant in all size changes, tests for pathway enrichment found 77 significantly enriched pathways, with 59 shown after filtering (removed pathways without 2 neighbors for simplicity). (**B**) Gene pathways clustered in 16 clusters GO-pathways based on gene similarity (**C**) Cluster 1 was the most enriched cluster (Enrichment Score 3.56; higher ES occurs with lower geometric mean of encompassed pathway p-values) containing four pathways; Insulin resistance, Longevity regulating pathway, AMPK signaling pathway, and Longevity regulating pathway-multiple species.

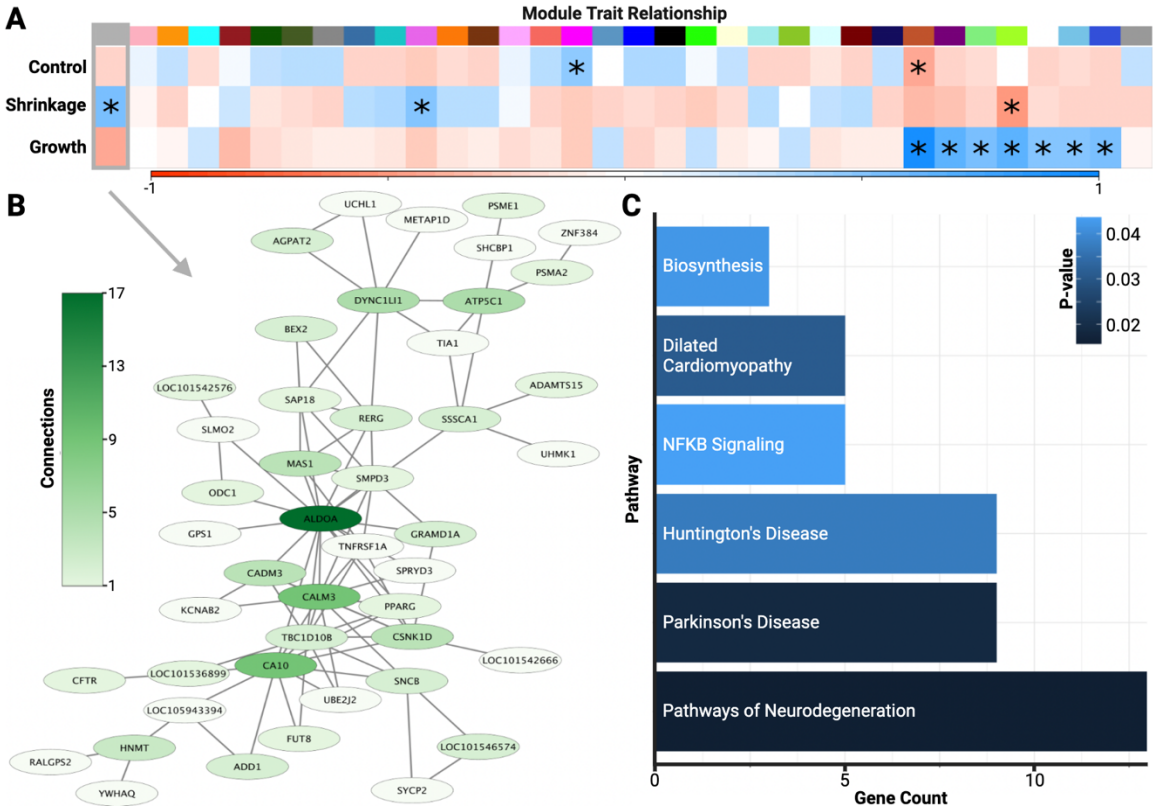

Figure 4. Gene network analyses across hippocampal size change. (**A**) Modules (34) of high gene co-expression in the hippocampus, including ten modules significantly correlated with target phenotypes (Regrowth, Shrinkage, and Control). The 346 gene grey module was the most significant module associated within the shrinkage phenotype (p = 0.01, r = 0.55). (**B**) Visualization of gene network (filtered and removed edges with weighted correlations < 0.02 and nodes with only a single neighbor). ALDOA was the most central to the network, with 17 connections to other nodes. (**C**) Pathway enrichment analysis also identified 6 pathways to be enriched for genes in the grey module: Pathways of Neurodegeneration, Parkinson's disease, Huntington's disease, NF-kappa beta Signaling, Dilated Cardiomyopathy, and Biosynthesis.